Trapping and mobilization of residual fluid during capillary desaturation in porous media

Lucian Anton[1,2] and R. Hilfer[2,3]
[1]*Institute for Atomic Physics, INFLPR, Laboratory 22, P.O. Box MG-7, 76900 Bukarest, Romania*
[2]*ICA-1, Universität Stuttgart, Pfaffenwaldring 27, 70569 Stuttgart, Germany*
[3]*Institut für Physik, Universität Mainz, 55099 Mainz, Germany*
(Received 21 April 1998; revised manuscript received 12 November 1998)

We discuss the problem of trapping and mobilization of nonwetting fluids during immiscible two-phase displacement processes in porous media. Capillary desaturation curves give residual saturations as a function of capillary number. Interpreting capillary numbers as the ratio of viscous to capillary forces the breakpoint in experimental curves contradicts the theoretically predicted force balance. We show that replotting the data against a novel macroscopic capillary number resolves the problem for discontinuous mode displacement. [S1063-651X(99)00304-9]

PACS number(s): 47.55.Mh, 81.05.Rm, 61.43.Gt, 83.10.Lk

I. INTRODUCTION

A displacement of one fluid by another within a porous medium poses challenging problems of microscale to macroscale transitions which have received considerable attention from physicists in recent years [1–20]. For reviews the reader is referred to [12,21]. Apart from the omnipresent quenched correlated disorder and structural heterogeneity, fluid-fluid and fluid-solid interactions generate metastability and hysteresis phenomena which have resisted quantitative prediction and understanding. A central problem of great practical importance is the prediction of residual nonwetting fluid saturation after flooding the pore space with immiscible wetting fluid [22–24]. Obvious interest in this problem arises from enhanced oil recovery [25,26] or *in situ* remediation of soil contaminants [27,28].

Microscopically the laws of hydrodynamics governing the pore scale processes are well known. The complexity of the microscopic fluid movements and the lack of knowledge about the microstructure and wetting properties, however, renders a detailed microscopic treatment impossible. Instead one has to resort to a more macroscopic treatment.

Desaturation experiments [29–36] show that the conventional macroscopic description is incomplete [23,24]. We shall begin our discussion by reminding the readers of this incompleteness. We then exhibit another problem [37]. This arises from the fact that microscopic capillary numbers seemingly cannot represent the force balance in a desaturation experiment.

Given these problems our main objective is to show that the recent analysis of [37] gives the correct force balance between macroscopic viscous and capillary forces for continuous mode desaturation experiments. For so-called discontinuous mode displacement it leads to bounds on the size of residual blobs.

II. PROBLEMS OF TWO-PHASE FLOW EQUATIONS

Let us begin our discussion with the standard macroscopic equations of motion for two-phase immiscible displacement. Macroscopic equations of motion describe multiphase flow on length scales large compared to a typical pore diameter. Hence they are applied to laboratory samples with linear dimensions on the order of centimeters as well as to whole reservoirs measuring kilometers and more. Consider a system having lengths L_x, L_y, L_z in the three spatial directions. The probe space is assumed to be filled with two immiscible fluids denoted generically as water (index w) and oil (index o). The equations read [38–40,37]

$$\phi \frac{\partial S_w}{\partial t} = \nabla \cdot \left\{ \frac{\mathbf{K} k_w^r}{\mu_w} [\nabla P_w - \rho_w g \mathbf{Oe}] \right\} \tag{1}$$

$$-\phi \frac{\partial S_w}{\partial t} = \nabla \cdot \left\{ \frac{\mathbf{K} k_o^r}{\mu_o} [\nabla (P_w + P_c) - \rho_o g \mathbf{Oe}] \right\} \tag{2}$$

and they are supplemented with the constitutive relationships

$$k_w^r(\mathbf{x},t) = k_w^r(S_n(\mathbf{x},t)), \tag{3}$$

$$k_o^r(\mathbf{x},t) = k_o^r(S_n(\mathbf{x},t)), \tag{4}$$

$$P_c(\mathbf{x},t) = P_c(S_n(\mathbf{x},t)), \tag{5}$$

where

$$S_n(\mathbf{x},t) = \frac{S_w(\mathbf{x},t) - S_{wi}}{1 - S_{wi} - S_{or}}. \tag{6}$$

The variables in these equations are the pressure field of water denoted as P_w and the water saturation S_w. The saturation is defined as the ratio of water volume to pore space volume. Pressures and saturations are averages over a macroscopic region much larger than the probe size, but much smaller than the system size. Their arguments are the macroscopic space and time variables $(\mathbf{x},t)$. The saturations obey $S_{wi} < S_w < 1 - S_{or}$, where the two numbers $0 \leqslant S_{wi}$, $S_{or} \leqslant 1$ ar two parameters representing the irreducible water saturation, S_{wi}, and the residual oil saturation, S_{or}. The residual oil saturation gives the amount of oil remaining in a porous medium after water injection. The normalized saturation S_n varies between 0 and 1 as S_w varies between S_{wi} and S_{or}. The permeability of the porous medium is given by the absolute (single phase flow) permeabil-

ity tensor **K**. The porosity ϕ is the volume fraction of pore space. The two fluids are characterized by their viscosities μ_w, μ_o and their densities ρ_w, ρ_o. The terms $\rho g \mathbf{Oe}$ represent the gravitational body force where $\mathbf{e}^T=(0,0,-1)$ is a unit row vector pointing along the negative z axis and g is the acceleration of gravity. The orthogonal matrix

$$\mathbf{O}=\begin{pmatrix} \cos\alpha_y & 0 & \sin\sigma_y \\ 0 & 1 & 0 \\ -\sin\alpha_y & 0 & \cos\alpha_y \end{pmatrix} \tag{7}$$

describes an inclination of the system. Here a rotation around the y axis with tilt or dip angle α_y was assumed. The macroscopic capillary pressure P_c is defined as the pressure difference between the oil and the water phase. The constitutive relation for P_c assumes that the capillary pressure function P_c depends only on the saturation [41]. In addition to P_c, the dimensionless relative permeabilities are assumed to be functions of saturation only, $k_w^r=k_w^r(S_w)$, $k_o^r=k_o^r(S_w)$. They represent the reduction in permeability for one phase due to the presence of the other phase [38,39]. The three constitutive relations $k_w^r(S_w)$, $k_o^r(S_w)$, and $P_c(S_w)$ are assumed to be known from experiment. Equations (1) and (2) are coupled nonlinear partial differential equations which must be complemented with large-scale boundary conditions. For laboratory experiments the boundary conditions are typically given by a surface source on one side of the sample, a surface sink on the opposite face, and impermeable walls on the other faces. For a geosystem the boundary conditions depend upon the well configuration and the geological modeling of the reservoir environment.

The problem with the macroscopic equations of motion (1) and (2) arises from the experimental observation that the parameters S_{or} and S_{wi} are not constant and known, but depend strongly on the flow conditions in the experiment [29–36,26]. Hence they may vary in space and time. More precisely, the residual oil saturation depends strongly on the microscopic capillary number $\mathrm{Ca}=\mu_w v/\sigma_{ow}$, where v is a typical flow velocity and σ_{ow} is the surface tension between the two fluids. The capillary desaturation curve $S_{or}(\mathrm{Ca})$ is shown in Fig. 1 for unconsolidated glass beads and sandstones [32,36]. Such curves contract clearly the assumption that the functions $k_w^r(S_w)$, $k_o^r(S_w)$, and $P_c(S_w)$ depend only on saturation. Instead they show that $k_w^r(S_w)$, $k_o^r(S_w)$, and $P_c(S_w)$ depend also on velocity [42,43] and pressure. Hence they depend on the solution and cannot be considered to be constitutive relations characterizing the system. The dependence shows that the system of equations of motion is incomplete.

The breakpoint in a capillary desaturation curve marks the point where the viscous forces, which attempt to mobilize the oil, become stronger than the capillary forces, which try to keep the oil in place. For this reason the capillary desaturation curves are usually plotted against Ca, which represents the microscopic force balance between viscous and capillary forces. From Fig. 1 it is seen that the theoretical force balance corresponding to $\mathrm{Ca}=1$ on the abscissa and the experimental force balances represented by the various breakpoints at $\mathrm{Ca}\ll 1$ differ by several orders of magnitude. Plotting residual saturation against the correct ratio of viscous to capillary forces should result in a breakpoint at $\mathrm{Ca}\approx 1$ [37,39].

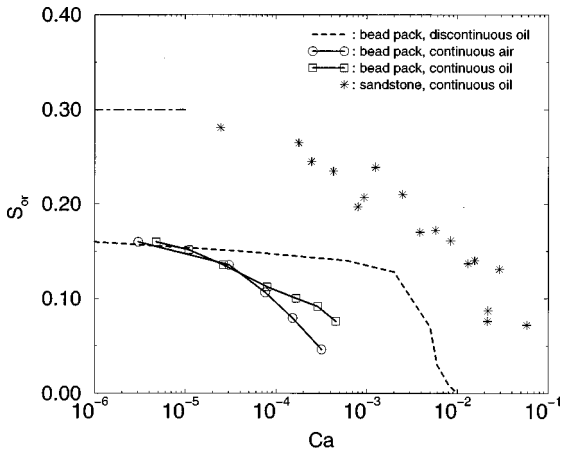

FIG. 1. Experimentally measured capillary desaturation curves (capillary number correlations) for bead packs [36] (solid lines with circles and squares) and sandstone [32] (star symbols) as a function of microscopic capillary number $\mathrm{Ca}=\mu_w v/\sigma_{ow}$. The dashed line is the desaturation curve for continuous mode displacement. The dash-dotted line marks the plateau value for sandstone.

We now proceed to show that a partial understanding of the macroscopic force balance can already be obtained from the traditional equations of motion. The main result of this analysis is a preliminary experimental validation of the dimensional considerations introduced in [37].

III. DISCONTINUOUS VERSUS CONTINUOUS MODE DISPLACEMENT

Before embarking on a discussion of the force balance during capillary desaturation, it is crucial to emphasize an important difference in the way capillary desaturation curves are measured.

(i) In the first method of measuring $S_{or}(\mathrm{Ca})$, the oil in a fully oil saturated sample is displaced with water at a very low Ca. After the oil flow at the sample outlet stops and several pore volumes of water have been injected without producing more oil, the flow rate is increased. Again the oil flow is monitored until no more oil appears at the outlet. In this way the flow rate is increased iteratively until S_{or} has fallen to zero. After the first injection the oil configuration is discontinuous (or disconnected) and it remains disconnected throughout the rest of the experiment. This mobilization mode will be called discontinuous.

(ii) In the second method of measuring capillary desaturation curves one again starts from a fully saturated sample, and performs a waterflood at a given value of Ca. After oil flow ceases at the outlet, the residual saturation is determined. Then the sample is again saturated fully with oil, a new value of Ca is chosen, and the injection is repeated. In this experiment the injection starts always with a connected oil phase contrary to the previous experiment, where the oil phase is discontinuous at higher Ca. This mobilization mode will be called continuous.

The capillary number required to reach a given S_{or} is known to be much lower in the continuous mode than in the discontinuous mode [36,35]. This is also seen in Fig. 1,

which shows continuous mode data and discontinuous mode data for the unconsolidated glass beads. From the fact that the equations of motion are only valid in the subinterval $S_{wi}<S_w<1-S_{or}$ it follows that they cannot be applied to discontinuous mobilization mode experiments. They should, however, be valid for the continuous mode to the extent that the equations themselves are correct. Therefore we discuss next the macroscopic force balance predicted by these equations from the continuous mobilization mode.

IV. MACROSCOPIC FORCE BALANCE

It was shown in [37] that the balance of macroscopic viscous and capillary forces is not represented appropriately by the microscopic capillary number Ca, and that a new macroscopic capillary number $\overline{\mathrm{Ca}}$ should be used instead. Here we generalize those results to anisotropic and inclined porous media and apply them to replot the S_{or} data obtained for the continuous mode displacement. To this end we rewrite Eqs. (1) and (2) in dimensionless form. Introducing the matrix

$$\mathbf{L}=\begin{pmatrix} L_x & 0 & 0 \\ 0 & L_y & 0 \\ 0 & 0 & L_z \end{pmatrix} \tag{8}$$

and defining l and $\hat{\mathbf{L}}$ through

$$l=(\det \mathbf{L})^{(1/3)}, \tag{9}$$

$$\mathbf{L}=l\hat{\mathbf{L}}, \tag{10}$$

one defines dimensionless quantities

$$\mathbf{x}=\mathbf{L}\hat{\mathbf{x}}=l\hat{\mathbf{L}}\hat{\mathbf{x}}, \tag{11}$$

$$\boldsymbol{\nabla}=\mathbf{L}^{-1}\hat{\boldsymbol{\nabla}}=(l\hat{\mathbf{L}})^{-1}\hat{\boldsymbol{\nabla}}. \tag{12}$$

Define k and $\hat{\mathbf{K}}$ through

$$\mathbf{K}=\begin{pmatrix} k_{xx} & k_{xy} & k_{xz} \\ k_{xy} & k_{yy} & k_{yz} \\ k_{xz} & k_{yz} & k_{zz} \end{pmatrix}, \tag{13}$$

$$k=(\det \mathbf{K})^{(1/3)}, \tag{14}$$

$$\mathbf{K}=k\hat{\mathbf{K}}. \tag{15}$$

The time scale is normalized as

$$t=\frac{L_xL_yL_z\phi\hat{t}}{Q} \tag{16}$$

using the volumetric flow rate Q. Time is measured in units of injected pore volumes. The pressure is normalized using the macroscopic equilibrium capillary pressure as [44,37]

$$P=P_b\hat{P}, \tag{17}$$

where

$$P_b=P_c[(S_{wi}-S_{or}+1)/2] \tag{18}$$

is the pressure at an intermediate saturation. $P_c(S_w)$ is the equilibrium capillary pressure function.

With these definitions the dimensionless macroscopic capillary numbers for oil and water, defined as

$$\overline{\mathrm{Ca}}_w=\frac{\mu_w Q}{P_b k l}, \tag{19}$$

$$\overline{\mathrm{Ca}}_o=\overline{\mathrm{Ca}}_w\frac{\mu_o}{\mu_w}, \tag{20}$$

give an expression of the balance between macroscopic viscous and capillary forces. The macroscopic gravity numbers

$$\overline{\mathrm{Gr}}_w=\frac{\mu_w Q}{\rho_w g k l^2}, \tag{21}$$

$$\overline{\mathrm{Gr}}_o=\overline{\mathrm{Gr}}_w\frac{\mu_o}{\mu_w}\frac{\rho_w}{\rho_o}, \tag{22}$$

express the viscous to gravity force balance. Finally the gravillary numbers

$$\overline{\mathrm{Gl}}_w=\frac{\rho_w g l}{P_b}, \tag{23}$$

$$\overline{\mathrm{Gl}}_o=\overline{\mathrm{Gl}}_w\frac{\rho_o}{\rho_w}, \tag{24}$$

express the ratio between gravitational and capillary forces. The well known bond number, measuring the magnitude of buoyancy forces, is given as

$$\mathrm{Bo}=\overline{\mathrm{Gl}}_w-\overline{\mathrm{Gl}}_o \tag{25}$$

in terms of the gravillary numbers.

With these definitions the dimensionless equations of motion may be rewritten as

$$\frac{\partial S_w}{\partial \hat{t}}=\hat{\boldsymbol{\nabla}}\cdot\{\hat{\mathbf{A}}k_w^r[\overline{\mathrm{Ca}}_w^{-1}\hat{\boldsymbol{\nabla}}\hat{P}_w-\overline{\mathrm{Gr}}_w^{-1}\hat{\mathbf{g}}]\}, \tag{26}$$

$$-\frac{\partial S_w}{\partial \hat{t}}=\hat{\boldsymbol{\nabla}}\cdot\{\hat{\mathbf{A}}k_o^r[\overline{\mathrm{Ca}}_o^{-1}\hat{\boldsymbol{\nabla}}(\hat{P}_w+\hat{P}_c)-\overline{\mathrm{Gr}}_o^{-1}\hat{\mathbf{g}}]\}, \tag{27}$$

where the dimensionless matrix

$$\hat{\mathbf{A}}=\hat{\mathbf{L}}^{-1}\hat{\mathbf{K}}\hat{\mathbf{L}}^{-1}=\begin{pmatrix} \frac{l^2k_{xx}}{L_x^2k} & \frac{l^2k_{xy}}{L_xL_yk} & \frac{l^2k_{xz}}{L_xL_zk} \\ \frac{l^2k_{xy}}{L_xL_yk} & \frac{l^2k_{yy}}{L_y^2k} & \frac{l^2k_{yz}}{L_yL_zk} \\ \frac{l^2k_{xz}}{L_xL_zk} & \frac{l^2k_{yz}}{L_yL_zk} & \frac{l^2k_{zz}}{L_z^2k} \end{pmatrix} \tag{28}$$

contains generalized ''aspect ratios.'' The vector

$$\hat{\mathbf{g}}^T=(\hat{\mathbf{L}}\mathbf{Oe})^T=\left(-\frac{L_x}{l}\sin\alpha_y,0,-\frac{L_z}{l}\cos\alpha_y\right) \tag{29}$$

TABLE I. The sample and flow parameters used in the calculations. The permeabilities for the glass bead packs were obtained using the relation between their radius and permeabilities published in [25] on p. 47. The capillary pressure was estimated using the Leverett-*j*-function correlation (30). For sandstone the *j* function from Ref. [51] was used and for bead packs the one from Ref. [50] was used. The *j* function was evaluated close to $(S_{wi}-S_{or}+1)/2$ according to Eq. (18).

Sample	Permeability k (10^{-12} m^2)	Porosity ϕ	Surface tension σ_{ow} (N/m)	Cap. pressure P_b (Pa)
sandstone 799 (Ref. [32])	0.14 (Ref. [32])	0.28 (Ref. [32])	3.37×10^{-2} (Ref [32])	1.7×10^{4} (Ref. [51])
70 μm bead pack (Ref. [36])	10 (Ref. [25])	0.36 (Refs. [25,53])	2.8×10^{-3} (Ref. [36])	2.4×10^{2} (Ref. [50])
115 μm bead pack (Ref. [36])	30 (Ref. [25])	0.36 (Refs. [25,53])	1.18×10^{-2} (Ref. [36])	5.8×10^{2} (Ref. [50])

represents the effect of dip angle and geometric shape of the system on the gravitational driving force.

V. APPLICATION TO EXPERIMENT

We are now in a position to plot the capillary desaturation curves against the macroscopic capillary number $\overline{\mathrm{Ca}}$, which represents the balance between macroscopic viscous and capillary forces. To do so we have searched the literature for capillary desaturation measurements and we found Refs. [22,25,29–31,45–48,35]. Unfortunately none of the publications contains all the necessary flow and medium parameters to calculate $\overline{\mathrm{Ca}}$. Measuring all the flow parameters for a displacement process is costly and time consuming, and hence they are rarely available (see also [49]). While permeability, porosity, and the fluid parameters such as viscosities and surface tensions are usually available capillary pressure data, relative permeabilities and residual saturations are not routinely measured. Hence we extract the required parameters from different publications assuming that they have been measured correctly and are reproducible anywhere and at all times. In spite of all the uncertainties, it is well known that the capillary pressure curves of unconsolidated sands with various grain sizes can be collapsed using the Leverett-*j* correlation [50,41,51]. The Leverett-*j* correlation states essentially that

$$P_c(S_w)=\sigma_{ow}\sqrt{\phi/k}\,j(S_w). \tag{30}$$

Often the formula contains in addition an average contact angle at a three-phase contact. We do not include the wetting angle as it is generally unknown, and including it would not change our results significantly. Similar to the capillary pressure data, the S_{or} data for unconsolidated sands seem to be well established [34,36] in spite of larger fluctuations of the results. Because most P_c and S_{or} data are available for unconsolidated sand and standard sandstones such as Berea or Fontainebleau, we limit our analysis to these two cases.

The experimental S_{or} data analyzed here are taken from Ref. [32] for sandstones and from Ref. [36] for unconsolidated glass beads. In Fig. 1 we show the capillary desaturation curve for oil-water displacement in a typical sandstone (sample No. 799 from [32]) using star symbols. These data were obtained in the continuous mode of displacement. The values of the surface tension and fluid viscosities for this experiment are given in Table I. We also show continuous mode S_{or} data for unconsolidated glass beads from Fig. 6 in 36. To calculate $\overline{\mathrm{Ca}}$ we have used the values given in Table I.

Plotting the data against $\overline{\mathrm{Ca}}$, we obtain Fig. 2. It is seen that the continuous mode displacements give a breakpoint for $\overline{\mathrm{Ca}}\approx1$ while the discontinuous mode displacements have their breakpoint at a higher value. This is consistent with the idea that the traditional equations of motion (1) and (2) should be applicable to the continuous mode but not to the discontinuous case.

The result obtained here is consistent with the theoretical predictions from [37]. To fully validate our use of $\overline{\mathrm{Ca}}$ as a correlating group for plotting continuous mode S_{or} data, however, it would be desirable to vary $\overline{\mathrm{Ca}}$ by varying the system size l. If the S_{or} curves obtained for different media and length scales l also show their breakpoint at $\overline{\mathrm{Ca}}\approx1$, this would give further evidence for the applicability of the traditional equations of motion. We consider it possible, however, that deviations appear indicating a breakdown of the equations also for continuous mode displacement [23,24].

As stated above, the equations of motion are not applicable to discontinuous mode displacements because of the constraint $S_{wi}<S_w<1-S_{or}$. Nevertheless we can use the group Ca to estimate an upper bound for the size of residual blobs. As the flow rate is increased, the residual blobs, whose size is so large that the viscous drag forces on them exceed the capillary retention forces, will break up and coalesce with

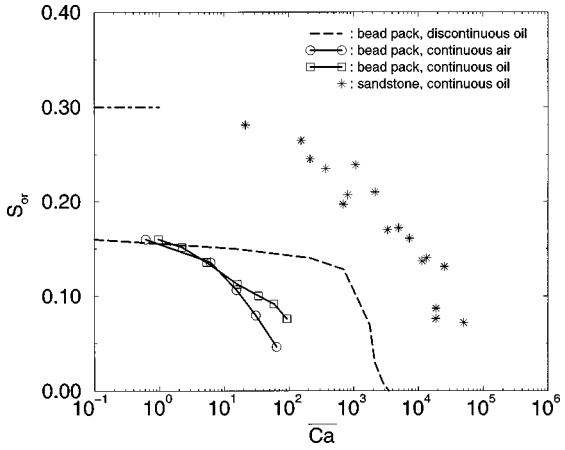

FIG. 2. Same as Fig. 1 but plotted against the macroscopic capillary number $\overline{\mathrm{Ca}}=\mu_w Q/(P_b k l)$ from Eq. (19). Note that the breakpoint for continuous mode displacement occurs around $\overline{\mathrm{Ca}}\approx1$.

other blobs which may again break up and coalesce further downstream [34,33]. The condition that the viscous forces dominate the capillary forces $\overline{\mathrm{Ca}} \geqslant 1$ predicts that after a flood with $\overline{\mathrm{Ca}}$ the porous medium contains only blobs of linear size smaller than

$$l_{\mathrm{blob}} \leqslant \frac{\mu_{\prime\prime} Q}{P_b k}. \tag{31}$$

This result is of importance for microscopic models [52] of breakup and coalescence during immiscible displacement.

ACKNOWLEDGMENTS

One of us (R.H.) thanks Dr. P. E. Øren for many useful discussions. We are grateful to the Deutsche Forschungsgemeinschaft for financial support.

[1] M. Blunt and P. King, Phys. Rev. A **42**, 4780 (1990).
[2] U. Oxaal, Phys. Rev. A **44**, 5038 (1991).
[3] U. Oxaal, F. Boger, J. Feder, T. Jøssang, P. Meakin, and A. Aharony, Phys. Rev. A **44**, 6564 (1991).
[4] R. Hilfer, Phys. Rev. B **44**, 60 (1991).
[5] R. Hilfer, Phys. Rev. B **45**, 7115 (1992).
[6] R. Hilfer, Phys. Scr. **T44**, 51 (1992).
[7] M. Blunt, M. King, and H. Scher, Phys. Rev. A **46**, 7680 (1992).
[8] V. Frette, J. Feder, T. Jøssang, and P. Meakin, Phys. Rev. Lett. **68**, 3164 (1992).
[9] P. Meakin, J. Feder, V. Frette, and T. Jøssang, Phys. Rev. A **46**, 3357 (1992).
[10] M. Kataja, K. Hiltunen, and J. Timonen, J. Phys. D **25**, 1053 (1992).
[11] B. Nøst, B. Hansen, and E. Haslund, Phys. Scr. **T44**, 67 (1992).
[12] M. Sahimi, Rev. Mod. Phys. **65**, 1393 (1993).
[13] M. Blunt and H. Scher, Phys. Rev. E **52**, 6387 (1995).
[14] V. Horvat and H. Stanley, Phys. Rev. E **52**, 5166 (1995).
[15] S. Schwarzer, Phys. Rev. E **52**, 6461 (1995).
[16] L. Furuberg, K. Maloy, and J. Feder, Phys. Rev. E **53**, 966 (1996).
[17] B. Virgin, E. Haslund, and R. Hilfer, Physica A **232**, 1 (1996).
[18] H. Kytömaa, M. Kataja, and J. Timonen, J. Appl. Phys. **81**, 7148 (1997).
[19] B. Berkowitz and H. Scher, Phys. Rev. Lett. **79**, 4038 (1997).
[20] J. Andrade, M. Almeida, J. M. Filho, S. Havlin, B. Suki, and H. Stanley, Phys. Rev. Lett. **79**, 3901 (1997).
[21] R. Hilfer, Adv. Chem. Phys. **XCII**, 299 (1996).
[22] G. Willhite, *Waterflooding*, Vol. 3 of *SPE Textbook Series* (Society of Petroleum Engineers, Richardson, TX, 1986).
[23] R. Hilfer, Phys. Rev. E **58**, 2090 (1998).
[24] H. Besserer and R. Hilfer (unpublished).
[25] L. Lake, *Enhanced Oil Recovery* (Prentice Hall, Englewood Cliffs, 1989).
[26] P. Øren, J. Billiotte, and W. Pinczewski, SPE Formation Eval. **March**, 70 (1992).
[27] J. Salles, J. Thovert, and P. Adler, J. Contam. Hydrol. **13**, 3 (1993).
[28] R. Helmig, *Multiphase Flow and Transport Processes in the Subsurface* (Springer, Berlin, 1997).
[29] H. Dombrowski and L. Brownell, Ind. Eng. Chem. **46**, 1207 (1954).
[30] J. Taber, SPE J. **9**, 3 (1969).
[31] J. Taber, J. Kirby, and F. Schroeder, AIChE Symp. Ser. **69**, 53 (1973).
[32] A. Abrams, SPE J. **15**, 437 (1975).
[33] I. Chatzis, M. Kuntamukkula, and N. Morrow, SPE Reservoir Eng. **August**, 902 (1988).
[34] N. Wardlaw and M. McKellar, Can. J. Chem. Eng. **63**, 525 (1985).
[35] R. Larson, H. Davis, and L. Scriven, Chem. Eng. Sci. **36**, 75 (1981).
[36] N. Morrow, I. Chatzis, and J. Taber, SPE Reservoir Eng. **August**, 927 (1988).
[37] R. Hilfer and P. Øren, Transp. Porous Media **22**, 53 (1996).
[38] A. Scheidegger, *The Physics of Flow Through Porous Media* (University of Toronto Press, Toronto, 1974).
[39] F. Dullien, *Porous Media-Fluid Transport and Pore Structure* (Academic, San Diego, 1992).
[40] M. Sahimi, *Flow and Transport in Porous Media and Fractured Rock* (VCH Verlagsgesellschaft mbH, Weinheim, 1995).
[41] J. Bear, *Dynamics of Fluids in Porous Media* (Elsevier, New York, 1972).
[42] P. deGennes, Europhys. Lett. **5**, 689 (1988).
[43] F. Kalaydijan, SPE Proc. **67**, 491 (1992).
[44] R. Hilfer and P. Øren, Tech. Report F&U-LoU-94001, Statoil A/S, Trondheim (1993).
[45] E. Donaldson, R. Thomas, and P. Lorenz, SPE J. **9**, 13 (1969).
[46] R. Ehrlich, H. Hasiba, and P. Raimondi, J. Petrol. **26**, 1335 (1974).
[47] E. L. duPrey, SPE J. **13**, 39 (1973).
[48] S. Gupta and S. Trushenski, SPE J. **19**, 116 (1979).
[49] R. Hilfer and P. Øren, Tech. Report F&U-LoU-96015, Statoil A/S, Trondheim (1993).
[50] M. Leverett, W. Lewis, and M. True, Trans. AIME **146**, 175 (1942).
[51] J. Dumore and R. Schols, SPE J. **26**, 437 (1974).
[52] L. Anton and R. Hilfer (unpublished first version of the manuscript).
[53] P. Wong, J. Koplik, and J. Tomanic, Phys. Rev. B **30**, 6606 (1984).